Environmental Science & Technology

Article

pubs.acs.org/est

Chemical and Mechanical Properties of Wellbore Cement Altered by CO_2-Rich Brine Using a Multianalytical Approach

Harris E. Mason,[†,*] Wyatt L. Du Frane,[†] Stuart D.C. Walsh,[†] Zurong Dai,[†] Supakit Charnvanichborikarn,[†] and Susan A. Carroll[†]

[†]Physical and Life Sciences Directorate, Lawrence Livermore National Laboratory, 7000 East Ave., Livermore, California 94551, United States

Supporting Information

ABSTRACT: Defining chemical and mechanical alteration of wellbore cement by CO_2-rich brines is important for predicting the long-term integrity of wellbores in geologic CO_2 environments. We reacted CO_2-rich brines along a cement-caprock boundary at 60 °C and pCO_2 = 3 MPa using flow-through experiments. The results show that distinct reaction zones form in response to reactions with the brine over the 8-day experiment. Detailed characterization of the crystalline and amorphous phases, and the solution chemistry show that the zones can be modeled as preferential portlandite dissolution in the depleted layer, concurrent calcium silicate hydrate (CSH) alteration to an amorphous zeolite and Ca-carbonate precipitation in the carbonate layer, and carbonate dissolution in the amorphous layer. Chemical reaction altered the mechanical properties of the core lowering the average Young's moduli in the depleted, carbonate, and amorphous layers to approximately 75, 64, and 34% of the unaltered cement, respectively. The decreased elastic modulus of the altered cement reflects an increase in pore space through mineral dissolution and different moduli of the reaction products.

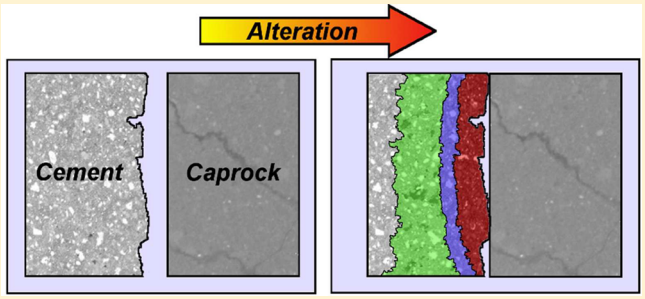

INTRODUCTION

Successful implementation of geologic CO_2 storage in deep saline and depleted oil reservoirs hinges on the long-term ability of wellbore cements to isolate gas and fluid flow between geologic strata, and prevent leakage along the wellbore and out of the storage reservoir.[1] Cement is highly reactive in carbon sequestration environments, which generate pH and chemical gradients across the cement that cause distinct reaction fronts to develop.[2−4] However, it is unclear what the impact of the alteration is on the long-term integrity of the cement in the wellbore environment, as cement alteration does not necessarily lead to enhanced permeability and leakage. A recent experimental study shows a mixed response of permeability over time when reacted with acidic fluids.[5] Detailed analysis of wellbore cement from a CO_2 enhanced oil recovery field indicated some leakage along surfaces adjacent to caprock and casing, but the overall performance of the cement to isolate reservoir fluids was not compromised.[6] The apparent reductions in permeability may reflect interplay between cement alteration and its mechanical response to in situ stress within the wellbore environment. Alteration of Portland cement by acids can significantly reduce the effective moduli making the reacted material significantly more compressible.[7,8] Cement alteration and the development of distinct reaction zones will likely also induce structural and mechanical changes that will impact transport of gas and fluid. Long-term assessment of wellbore performance to isolate CO_2 reservoir fluids will use advanced models that couple chemical, mechanical, and transport processes to represent the range of relevant parameters in the field that cannot be fully captured by experiment. Experiments can be used to define key processes and parameters that form the basis of the advanced simulations.[9,10]

One pathway for escape of CO_2 from the wellbore is along fractures between the cement and the reservoir caprock. The results presented here represent a portion of the work we have been conducting to understand the consequences of cement alteration on wellbore permeability along fractures at the cement-caprock interface. The objective of this work was to 2-fold: (1) to provide a cement alteration model that ties reaction pathway to the mechanical response of the alteration zones based on new data collected from a fracture flow experiment; and (2) to discuss the implications of these findings to wellbore performance in carbon storage environments. We collected a detailed, spatially resolved data set to constrain the reaction pathways and structural changes occurring during the reaction of wellbore cements. Cement alteration reactions were identified from solid-state nuclear magnetic resonance (NMR) spectroscopic analyses, scanning electron microscopy

Received: October 1, 2012
Revised: December 13, 2012
Accepted: January 4, 2013
Published: January 4, 2013

   dx.doi.org/10.1021/es3039906 | Environ. Sci. Technol. 2013, 47, 1745−1752

(SEM), powder X-ray diffraction (XRD), and changes in solution chemistry. Chemically induced geomechanical changes were identified by spatially resolved nanoindention and macroscopic loading measurements.

METHODS

Reaction of Wellbore Cement with CO_2 Saturated Brine. We reacted cured Class G Portland cement with CO_2 saturated brine in two different flow-through systems to generate samples representative of CO_2 leakage in the wellbore environment. Details of the cement curing conditions and preparation are provided in the Supporting Information. The core flood experiment followed the procedures outlined by Smith et al.,[11] and used a sample core (15 mm diameter, 37 mm length) that was half cement−half caprock with a planar aperture between the two materials. The caprock half used was a fully dense calcite cemented, quartz-sandstone sourced from an oil wellbore in Kern County, California at a depth of 4245 m (13 927 ft). A pathway between the two flat surfaces was generated by abrading the cement surface with glass beads prior to joining the two halves with an estimated 15 μm aperture. This method differs from that used in our other work where masking was used to achieve a larger and more uniform aperture.[12] Experimental pressure, temperature, initial brine chemistry, and partial pressure CO_2 (pCO_2) are representative of those from CO_2-EOR fields.[11] The core was maintained at a confining pressure ($P_{confine}$) of 24.8 MPa and 60 °C. Brine (Table S1 of the Supporting Information) was maintained at 60 °C in a separate pressure vessel and saturated with either 0 or 3 MPa pCO_2 to generate conditions that were near equilibrium or undersaturated with calcite and dolomite, respectively. Brine was injected through a hastelloy frit into the core with an average flow rate of 0.05 cm^3/min with pore pressure fixed to 12.4 MPa at the outlet by a back pressure regulator. The core was equilibrated with CO_2 free brine for 7 days prior to reaction with brine that contained pCO_2 = 3 MPa for an additional 7 days. Previous work has shown that CO_2 saturation or equilibration with the fluid generally occurred within 8 h.[13] In situ measurements of the inlet pressure (P_{inlet}) and outlet pressure (P_{outlet}) were used to calculate differential pressure across the sample ($\Delta P = P_{inlet} - P_{outlet}$) and pore pressure ($P_{pore} = \Delta P/2$)). $P_{confine}$ and P_{outlet} were varied in the first and last days of reaction to test the geomechanical response of the fracture (Supporting Information). No precipitated material was observed at the inlet or outlet after the reaction. The reacted sample was stored in a sealed plastic bag at ambient temperatures prior to analysis. Reacted output brine was periodically sampled and aliquots submitted for total inorganic carbon (TIC), inductively coupled plasma mass spectrometry (ICP−MS) and ion chromatography (IC) analyses. Speciation calculations were made from the measured solution chemistry with eq 3 and the Yucca Mountain (V8) thermodynamic database in which solution pH was calculated from charge balance.[14] After reaction, a total of nine subsamples from a section of the reacted cement half core were taken using careful grinding of the core with fine tweezers and steel rasp. The weights of the resulting powders were recorded and samples were analyzed by powder X-ray diffraction (XRD) from 10 to 50° 2θ using a Bruker D8 Advance X-ray diffractometer, and solid-state NMR spectroscopy (Supporting Information). A second section of the same core was used for for nanoindention and scanning electron microscopy (SEM) measurements (Supporting Information).

We also conducted a flow through experiment[13] to react a larger volume of cement for use in additional NMR experiments requiring more material. The brine was maintained in a separate mixer pressure vessel at 60 °C with pCO_2 = 3 MPa. The cement was equilibrated for 24 h with CO_2-free brine before the CO_2 saturated brine was injected through the inlet of the reactor vessel at a rate of 0.10 cm^3/min for 7 days, with total pressure fixed at 6.5−7.0 MPa by back-pressure regulator at the outlet.

RESULTS AND DISCUSSION

Spatially Resolved Analysis of Wellbore Cement Carbonation. The reactions of the cement with CO_2 saturated brine produce three distinct alteration zones parallel to the initial cement−caprock interface that can be clearly observed by SEM analysis of the core flood sample (Figure 1). These

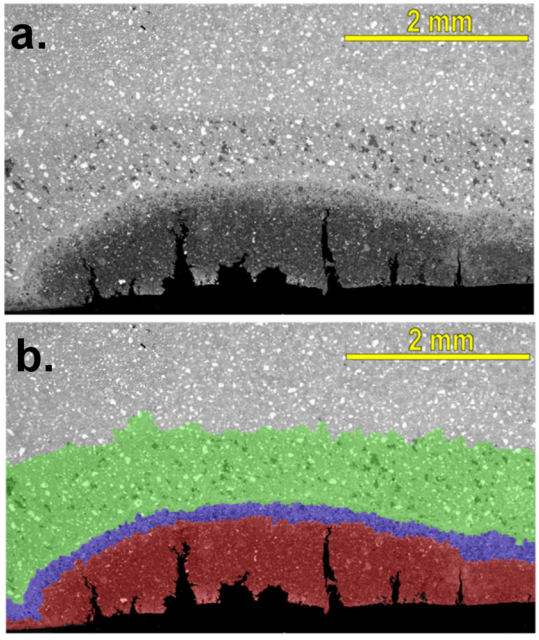

Figure 1. Backscattered SEM images of the central portion of the core flood sample. (a) Original SEM image. (b) The results of image segmentation are presented as colored overlays on the original image to highlight the reaction zones. Red: Amorphous layer. Blue: Carbonate layer. Green: Depleted layer. This figure is representative of the typical reaction extent throughout the core.

regions are similar to those previously described by Kutchko and co-workers in which hardened cement was altered in CO_2 saturated brines (1% NaCl) in batch reactors for up to 9 days.[2−4] Accordingly, we will adopt a similar naming scheme when discussing these layers throughout this study. The first layer (red in Figure 1B) will be referred to as the amorphous layer and has an average thickness of 930 μm, the second (blue in Figure 1B) is the carbonate layer and averages 190 μm thick, and the final layer (green in Figure 1B) is the depleted region and has an average thickness of 650 μm. The remainder of the core is unaltered cement. The alteration layers and their average thicknesses have been defined using image segmentation methods. The total extent of reaction in this sample is ~2 mm, and is on average thicker than those previously observed.[2−4] The remainder of the 7 mm diameter core appears unaffected by these reactions and is denoted as unaltered cement.

dx.doi.org/10.1021/es3039906 | Environ. Sci. Technol. 2013, 47, 1745−1752

Further information about the reactions that occur in these layers can be gained from sequential sampling and analysis of these layers as a function of reaction depth. The XRD results provide information about how the crystalline phases in these samples are changing (Figure 2). The unreacted cement

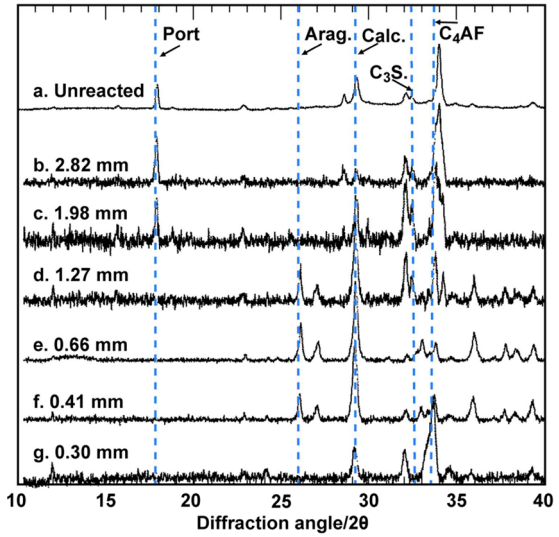

Figure 2. Powder X-ray diffraction patterns for (a) unreacted cement and (b–f) sequentially sampled sections of core-flood altered cement sample. Measurements in mm are given for the depth of sampling from the fracture surface. Blue lines denote the position of the most intense reflection for the phases portlandite (Port.), aragonite (Arag.), calcite (Calc.), tricalcium silicate (C_3S), and brownmillerite (C_4AF). Additional peaks from these phases are unlabeled, but may overlap with the labeled peaks. XRD patterns have been normalized such that the most intense peak in each pattern is the same height.

contains portlandite, Ca_3SiO_5 (alite; C_3S) and the calcium aluminate phase brownmillerite (C_4AF) as the dominant crystalline phases (Figure 2a). We can track changes in the relative abundances of these phases as the reaction progresses. We observe distinct layers that are marked by disappearance of portlandite and C_3S (Figure 2d), the emergence of calcite and aragonite (Figure 2d–f), and finally the dissolution of these carbonate phases. Given the minor reflections from C_4AF in all but the final layer, it is clear that only residual amounts of crystalline calcite reside within this layer (Figure 2g). A summary of the mineral phases identified in this study are given in Table S2 of the Supporting Information.

Given that the majority of the minerals present in hardened Portland cement are poorly crystalline or amorphous,[15] the XRD results alone cannot fully trace all the reactions occurring in this system. We used ^{29}Si and ^{27}Al NMR spectroscopy to provide information on the alteration of these phases (Figure 3). The ^{29}Si NMR data supplies information about the C_3S and amorphous calcium silicate hydrate (CSH) phases, which represent the majority of the cement.[15] The peak at −74 ppm arises from residual C_3S clinker material and the two peaks at −82 and −87 ppm result from the Q^1 and Q^2 silica sites in the CSH phase, respectively (Figure 3a).[16] We observe that in the least reacted regions (Figure 3a,b; as indicated by SEM and XRD) there is little change in the collected NMR spectra. However, as the reaction fronts progress we see a rapid loss of structure beginning at the edge of the carbonate zone (Figure 3c) and a complete loss of structure through the carbonate layer (Figure 3d) and into the amorphous layer (Figure 3e). Comparison of the XRD and NMR suggests that the Ca-leaching of the CSH occurs simultaneously with the formation of calcium carbonate.

As the alteration of the cement progresses, the Al environment changes from being dominated by octahedrally coordinated Al ($Al^{[6]}$; Figure 3f) to tetrahedrally coordinated Al ($Al^{[4]}$; Figure 3j). Minor amounts of $Al^{[4]}$ observed in the least reacted samples (Figure 3f) likely represent Al in CSH minerals.[17,18] The major change observed indicates a shift from a $Al^{[6]}$ dominant phase such as an oxide or sulfate to a $Al^{[4]}$ dominant phase such as an aluminosilicate. The $Al^{[6]}$ is likely contained in Al-sulfate phases,[19] since $Al^{[6]}$ in Ca-ferrite phases cannot be observed in ^{27}Al NMR experiments due to their high Fe content.[20] The increase in the Al signal intensity of the spectra collected for the amorphous layers (Figure 3j) likely occurs from the dissolution of Fe-rich phases and incorporation of Al into silicate phases.

Geomechanical Characterization. Geochemical alteration by CO_2-saturated brine significantly weakened the cement. The differential pressure data (ΔP) was used to make a parallel plate approximation of hydraulic aperture (b):

$$b = \left(\frac{12Q\mu l}{\Delta P w}\right)^{1/3} \quad (1)$$

where Q is flow rate, μ is the temperature-dependent dynamic viscosity of the brine (4.67×10^{-4} kg/m/s), l is the core length, w is the core diameter.[21] Average normal stress across the fracture plane can be approximated as $P_{confine} - P_{pore}$, and was varied by making alternating changes to $P_{confine}$ and P_{outlet} at the beginning and end of the experiment. The hydraulic aperture reduced by a factor of ∼3, and was more sensitive to changes in normal stress after the alteration (Figure 4).

The individual hardness and Young's moduli values measured across the reaction zones by nanoindentation exhibit a large degree of scatter that reflects the heterogeneity at the micrometer scale within each layer (Figure 5). The average values for hardness agree with those reported previously for reaction zones in carbonated cement (Figure 5a).[4] The average Young's moduli decreased across the reaction zones from 28 ± 7 GPa in the unaltered cement, to 21 ± 6 GPa in the depleted layer, to 18 ± 3 GPa in the carbonate layer, and finally to 9.6 ± 1.0 GPa in the amorphous layer (Figure 5b). The final layer lies closest to the fracture surface and exhibits significantly less compressive strength than the others. Ultrasonic measurements on two pristine cement cores and compressive load testing on third core measured an average Young's modulus of 19 GPa and are slightly lower than that obtained by nanoindentation for the unreacted layer. The nanoindentation measurements were performed on a dry sample, and the presence of H_2O could alter the mechanical values, particularly for the amorphous layer which would have been weaker in the wet sample.[22]

Characterization of the Amorphous Cement Layer. It has been largely assumed that the end product of the alteration reactions with CSH is amorphous silica based largely on mass balance calculations. We employed additional NMR measurements to identify the major mineral constituent of the amorphous layer as an amorphous aluminosilicate. This result is reasonable since Mg-aluminosilicates have been previously found to replace Ca-silicate grains in naturally altered cement.[23,24]

dx.doi.org/10.1021/es3039906 | Environ. Sci. Technol. 2013, 47, 1745–1752

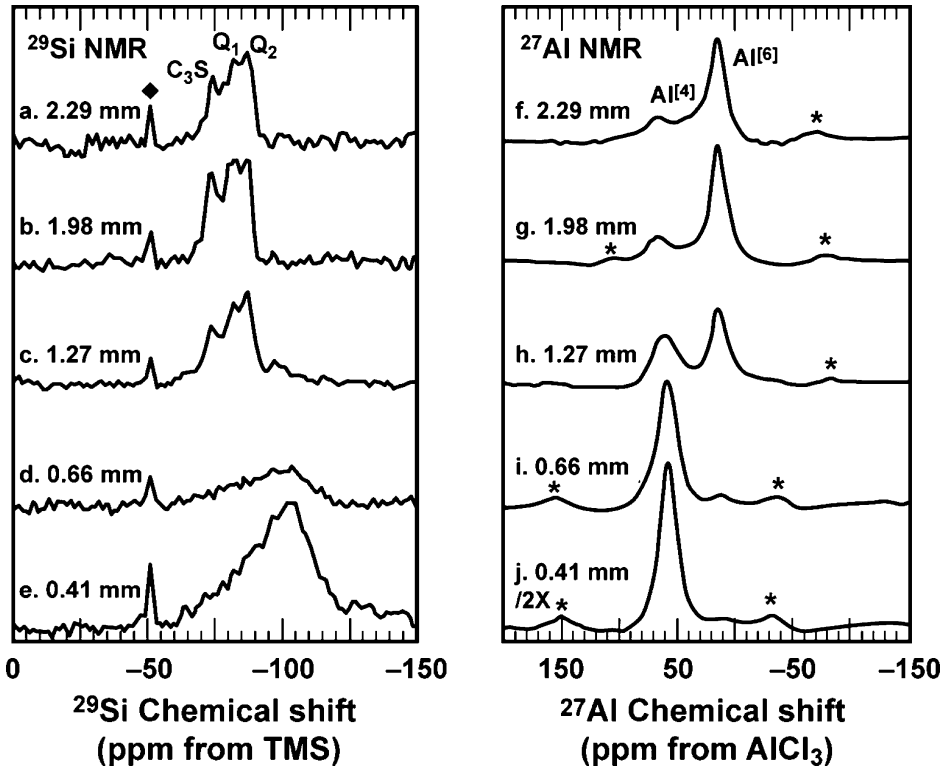

Figure 3. Stacked NMR plots of sequentially sampled cement from the core-flood experiment. (a–e) ^{29}Si NMR spectra. Peaks associated with C_3S and Q^1 and Q^2 peaks of CSH are labeled and diamond identifies background peak from SiN rotor. (f–j) ^{27}Al NMR spectra. Peaks identified are identified as occurring from $Al^{[4]}$ and $Al^{[6]}$. Bottom ^{27}Al NMR spectrum is downscaled by a factor of 2X. Asterisks mark the location of spinning sidebands.

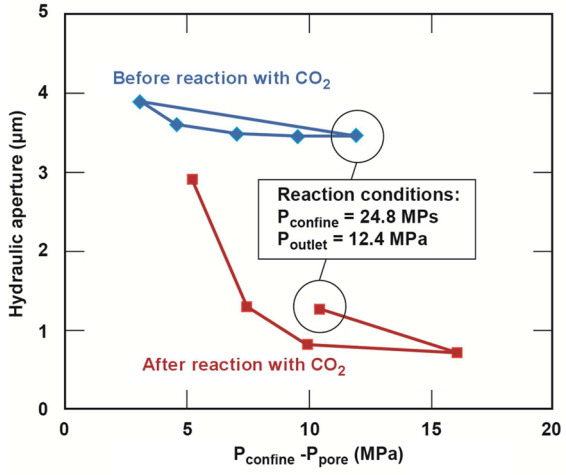

Figure 4. Hydraulic aperture (b, calculated using eq 1) response to variable stress ($P_{confine} - P_{pore}$) before (blue diamonds) and after (red squares) cement reaction with brine containing CO_2. Data was collected continuously and are plotted as average values after each change in pressure. The hydraulic aperture decreased from 3.5 to 1.3 μm over the course of the reaction at fixed $P_{confine}$ = 24.8 MPa and P_{outlet} = 12.4 MPa. The aperture response is relatively smaller, linear, and exhibits less hysteresis before the CO_2-cement reaction than after.

Important information about phase identity can be gleaned from the hydration state.[25] We gathered such information from ^{1}H SP/MAS, ^{27}Al{^{1}H} REDOR, and ^{29}Si{^{1}H} CP/MAS NMR measurements of the amorphous layer. First, we observed that the ^{1}H NMR spectrum collected at 55 kHz produces only a single peak at 4.8 ppm with a strong sideband pattern characteristic of structural water molecules (Figure S1 of the Supporting Information).[26] Absent were peaks from structural hydroxyls that occur between 0 ppm and 2 ppm.[26] ^{29}Si{^{1}H} CP/MAS NMR can be used to enhance the observed ^{29}Si signal from ^{1}H polarization transfer from abundant silanol protons.[27] However, we observed a significant decrease in the intensity of the ^{29}Si{^{1}H} CP/MAS spectra when compared to SP/MAS spectra (Figure S2 of the Supporting Information) that indicates that either only a small subset of silanol groups exist or more likely that the polarization transfer from structural waters is inefficient at enhancing the observed signal. If this phase is amorphous silica, then we would expect an enhancement of the CP/MAS signal compared to the SP/MAS spectrum. These observations are supported by the ^{27}Al{^{1}H} REDOR experiment which can be used to constrain the identity of aluminosilicate phases.[25] We also analyzed a series of representative minerals that contain $Al^{[4]}$ species, and a range of Al–H environments which could be expected to form under the conditions of the experiment. The measured REDOR dephasing curve for the amorphous layer is similar to the zeolite phase mordenite which contains mobile structural waters (Figure 6). This contrasts that for the zeolite analcime and the clay beidellite that contain rigidly bound proton species. The mobility of the water quenches the dipole coupling and explains both the decrease in the REDOR dephasing and the decreased signal intensity for the ^{29}Si{^{1}H} CP/MAS NMR spectrum.

Geochemical speciation calculations of the output solution chemistry were consistent with the above solid analysis. Geochemical alteration of the cement and caprock by CO_2-rich brine buffers the solution pH from pH 4.3 to pH 4.97 ±

dx.doi.org/10.1021/es3039906 | Environ. Sci. Technol. 2013, 47, 1745–1752

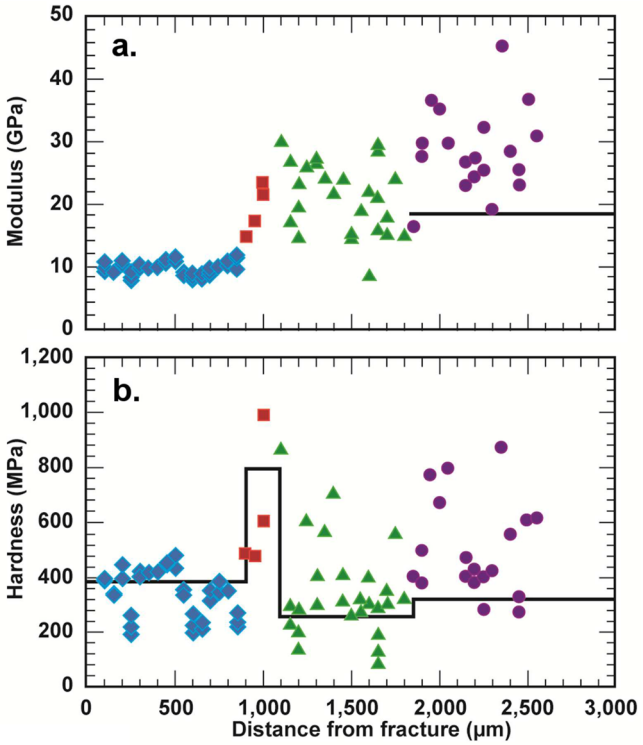

Figure 5. Nanoindentation measurements on core-flood experiment sample of (a) Young's modulus and (b) hardness in transect across each reaction zone: amorphous (blue diamonds), carbonate (red squares), depleted cement (green triangles), and unreacted cement (purple circles). (a) Average ultrasonic, load measurements of Young's modulus (19 GPa, this study) of unreacted cement and (b) hardness measurements for these layers in experiments by Kutchko et al.[4] are plotted as solid lines for comparison.

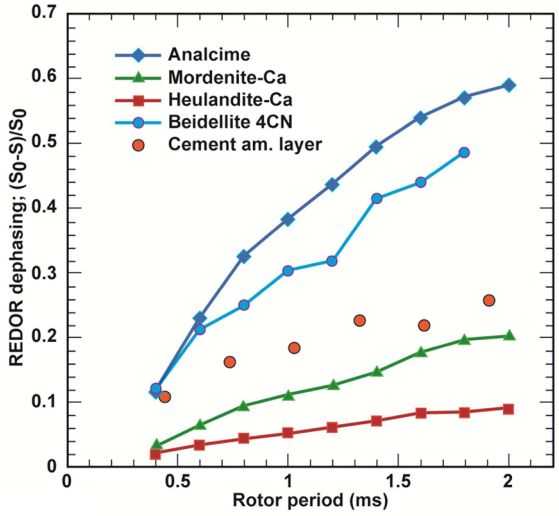

Figure 6. $^{27}Al\{^{1}H\}$ REDOR NMR results for various aluminosilicate minerals containing $Al^{[4]}$ and the amorphous cement layer. Since beidellite contains both $^{[6]}Al$ and $^{[4]}Al$, only the results for $^{[4]}Al$ peak are presented. Lines are present only to guide the eye.

0.04 and yields output solutions that were in equilibrium with calcite (log SI −0.09 ± 0.06) and anhydrite (log SI −0.09 ± 0.01), supersaturated with respect to crystalline mordenite (log SI 1.32 ± 0.11), and undersaturated with amorphous silica (log SI −0.56 ± 0.02). Additionally, the output solutions had the same CO_2 content as the input solution (pCO_2 =3.1 ± 0.2), as would be expected for flow along a short fracture. Saturation indices were calculated from 5 to 142 h (Figure 7). The solution compositions suggest that the solubility of the amorphous zeolite identified by NMR is slightly more soluble than its crystalline reference shown here and less soluble than commonly invoked amorphous silica (although true solubility would require reversed experiments that approach equilibrium from super and undersaturation).

The core-flood experiment samples were allowed to dry at ambient conditions and shrinkage cracks developed in the amorphous layer that coated the reacted samples (c.f. Figure 1). These features could develop through the loss of structural water in the amorphous aluminosilicate or through loss of pore water. The loss of structural water could substantially change the structure of the amorphous material, and manifest as distinct changes in the ^{29}Si NMR spectra. We, therefore, collected ^{29}Si spectra of flow through samples immediately after the experiment was brought down when the layer was still wet, and after the sample had been dried in a 50 °C oven overnight. We observe no changes in the spectra of these samples, and conclude the shrinkage cracks do not result from substantive structural changes, but rather the loss of pore water. This conclusion is supported by a prior study that attributed such features to expulsion of water from the amorphous layer via syneresis.[28]

On the basis of the above results, we assign the majority amorphous component to an amorphous aluminosilicate of similar composition to the zeolite minerals mordenite or clinoptilolite. The difference between these two minerals is largely structural. We cannot differentiate between the two with the current analytical methods, nor is it appropriate to assign a specific crystalline structure since this amorphous material by definition lacks long-range structural order. However, this phase is metastable and could be expected to transform to a thermodynamic endmember.

Revised Geochemical Pathways. Previous models suggest these layers form first through the dissolution of portlandite, followed by the precipitation of Ca-carbonate, and finally the leaching of Ca from silicates to form amorphous silica after the Ca-carbonates have dissolved.[2,3] The largest differences in our model compared to that previously proposed is that alteration of CSH occurs concurrently with Ca-carbonate precipitation and that the final alteration phase is an amorphous zeolite and not amorphous silica. We will discuss the proposed cement alteration reactions in detail as they relate to the three discrete reaction zones observed (Figure 8).

At the boundary of the unaltered and depleted zones, pH gradients produced from these reactions cause portlandite to dissolve and initially supply dissolved Ca^{2+} to the system, without significant precipitation of Ca-carbonate.

$$Ca(OH)_2 \rightarrow Ca^{2+} + 2OH^- \quad (2)$$

Any alteration of the CSH in the depleted layer appears to be negligible based on the absence of the amorphous aluminosilicate reaction product as detected by NMR.

At the boundary of the carbonate and depleted zones, the presence of carbonic acid triggers a series of linked reactions causing calcium−aluminum−monosulfate and CSH to dissolve.

$$Ca_4Al_2O_6(SO_4) + 12H^+ \leftrightarrow 4Ca^{2+} + 2Al^{3+} + SO_4^{2-} + 6H_2O \quad (3)$$

dx.doi.org/10.1021/es3039906 | Environ. Sci. Technol. 2013, 47, 1745−1752

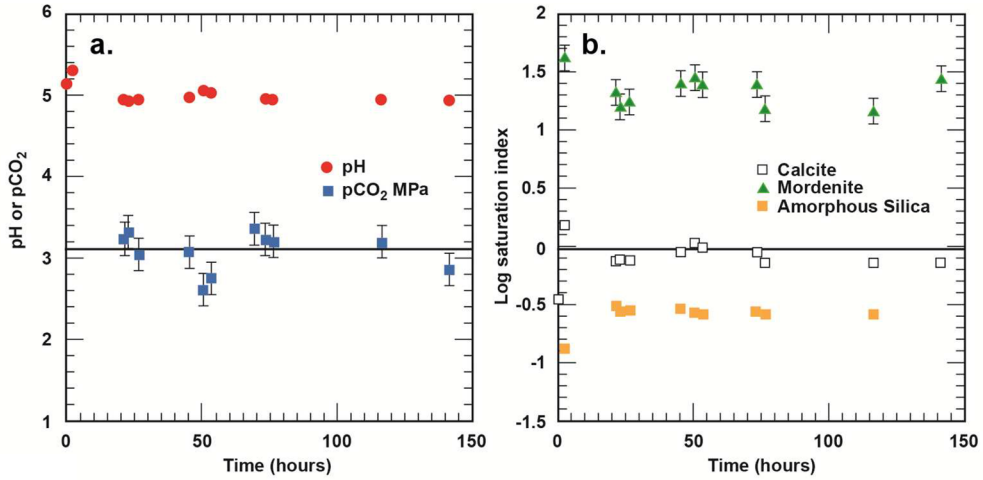

Figure 7. (a) Output solution pH, pCO_2, and (b) mineral saturations plotted as log SI vs time for calcite, mordenite, and amorphous silica. Averaged values reported in the main manuscript reflect steady-state values averaged after 23 h of reaction.

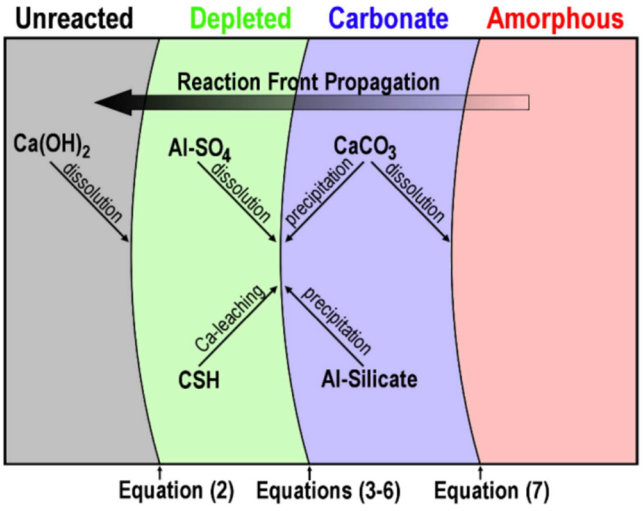

Figure 8. Schematic representation of the main reactions and their location with respect to the development of the alteration zones. The arrows are used to indicate the boundary where the reactions are occurring. The equations refer to those which occur at the reaction front and are detailed in the text.

$$Ca_6Si_5O_{14}(OH)_4 + 12H^+ \leftrightarrow 6Ca^{2+} + 5SiO_2(aq) + 8H_2O \quad (4)$$

The composition of the CSH phase has a Ca:Si ratio of 1.2 and approximates the general chemical formula used above based on a detailed study of well-defined CSH phases that correlates Q^1:Q^2 abundances to Ca:Si ratios.[16] The water content in the mass balance equations is difficult to constrain because it is not possible to obtain the structural water content of the CSH within the current heterogeneous cement sample using the current analytical methods.

The dissolution reactions 3 and 4 result in calcite, aragonite, and amorphous aluminosilicate precipitation:

$$Ca^{2+} + HCO_3^- \rightarrow CaCO_3 + H^+ \quad (5)$$

$$0.2895Ca^{2+} + 0.361Na^+ + 0.94Al^{3+} + 5.06SiO_2(aq) + 5.348H_2O \rightarrow Ca_{0.2895}Na_{0.361}Al_{0.94}Si_{5.06}O_{12} \bullet 3.468H_2O + 3.76H^+ \quad (6)$$

The leaching of Ca from CSH phases consumes Na^+ from the brine and the dissolved Al^{3+} to form an amorphous zeolite modeled here as mordenite. Mechanistically we do not know if alteration of CSH to zeolite occurs through dissolution and precipitation as described above, or through structural reorientation caused by the diffusion of Na and Al for Ca. In either case, the reaction can be modeled with eqs 2−6. The completion of the above reactions also results in the hydration of residual anhydrous clinker materials. Ca-aluminates react with water and available sulfate sources to form additional Ca−Al-sulfates to feed dissolution reactions.

$$Ca_3Al_2O_6 + 3Ca^{2+} + 3SO_4^{2-} + 32H_2O \rightarrow Ca_6Al_2O_6(SO_4)_3 \bullet 32H_2O \quad (7)$$

Anhydrous C_3S reacts with water to form additional CSH phases for the leaching reactions.

$$5Ca_3SiO_5 + 11H_2O \rightarrow Ca_6Si_5O_{14}(OH)_4 + 9Ca(OH)_2 \quad (8)$$

These reactions produce complex feedback loops, which continue until the clinker materials have been fully consumed by the alteration reactions.

At the final boundary between the carbonate and amorphous zones, Ca-carbonate phases dissolve due to strong pH gradients from the CO_2-rich brine. Ca-carbonate dissolution results in a substantial amount of pore space that is taken up by water.

The reactions involving Al are important given the influence that even small amounts of Al can have on the precipitation and dissolution of silicate minerals,[29−31] but have been largely overlooked in cement reactions. The ^{27}Al NMR data showing that the alteration induces a change from $Al^{[6]}$ sulfate minerals to $Al^{[4]}$ silicate minerals. This finding is counter to prior assumptions that Al should partition into $Al^{[6]}$-oxides/hydroxides.[15] The feedback loop proposed is supported by the ^{27}Al spectra collected for the amorphous layer, which show a large increase in the spectral intensity relative to the unreacted layers. These data suggest that previously "invisible"

dx.doi.org/10.1021/es3039906 | Environ. Sci. Technol. 2013, 47, 1745−1752

Al has dissolved from the Fe-rich Ca-aluminate phases and partitions into the amorphous aluminosilicates.

There are two significant differences between our results and from those of previous studies of wellbore cement reaction. Most notably, we observe the development of larger reaction zones (~2 mm) over a shorter experimental duration (8 days). Studies by Kutchko et al. presented the results of batch alteration experiments where small (500 μm) reaction zones emerged after 9 days of reaction.[2,3] Similarly, work by Carey et al. observed only 50 to 150 μm of alteration after 16.6 days of reaction.[32] The more extensive reaction zones observed in our experiments may reflect difference in design where the brine is continually replaced and does not have the potential to reach equilibrium with the alteration products as it could in a batch setup. Geochemical modeling of cement alteration indicates sensitivities to not only the brine chemistry and initial mineralogical composition of the cements, but also physical parameters such as tortuosity and permeability.[12]

The geochemical model presented above attempts to more completely capture all of the reactions that occur during cement alteration. In addition to added reaction pathways, it significantly modifies the existing models for the transport of Ca in the system. In the model of Kutchko et al,[2,3] the formation of the Ca-carbonate layer was understood to protect the Ca-silicate materials from leaching reactions, and leaching only occurred after these carbonate minerals were dissolved. Our analytical results suggest that Ca-leaching is concurrent with the formation of Ca-carbonate minerals. The alteration of the silicates is evidenced by the loss of distinct peaks for CSH and C_3S in the ^{29}Si NMR spectra (Figure 3d) as well as the absence of C_3S peaks in XRD patterns (Figure 2d–f) collected for carbonate layer subsamples. Backscattered SEM images also show substantial amounts of dark grains (indicating a loss of higher atomic weight elements) with similar morphology to the silicate grains within this carbonate zone that result from the loss of Ca (Figure S3 of the Supporting Information).

Implications for Wellbore Stability. We have identified key geochemical reactions and geomechanical properties for the alteration layers that result from cement reactions with CO_2-rich brines representative of carbon storage environments. This data can provide the basis for coupled chemical–mechanical–flow models[12] to evaluate the long-term stability of wellbores used in CO_2 sequestration activities. Thermodynamic properties needed to assess porosity changes in the absence of in situ stresses are available for portlandite, calcite,[33] and cement minerals,[33,34] but data for the amorphous zeolite are not. Comparison of the standard state molecular volumes for CSH (107.10 cc/mol-Si[33]) and crystalline mordenite (41.01 cc/mol-Si[35]) suggest a significant increase in pore volume when the CSH is altered to the amorphous zeolite. The estimated pore volume change would be even greater if the alteration product were to be modeled as amorphous silica (29.0 cc/mol-Si[33]). The decrease in permeability over the course of our experiments and the nanoindentation data indicate that the altered layers compress as a consequence of reaction limiting the impact of the chemical alteration on fluid transport. Although applied stresses in the field are likely to differ from those in our experiments, the ex-situ moduli measured here can be calibrated against the in situ pressure changes to ensure their applicability to large-scale simulations of wellbore integrity.

Cement alteration dominates the geochemical reactions at the cement–caprock interface and was the focus of this work. However, caprock alteration will also contribute to permeability evolution. In our more expansive experimental data set (not shown here), the input brine partially dissolved calcite present in the tight sandstone caprock, helping to buffer pH and locally increasing porosity. Carbonate mineral dissolution at the caprock interface is likely to occur in all wellbore settings because the carbonate minerals are ubiquitous in sedimentary rocks. Wellbore cement in contact with clay-rich shale caprocks may also result in smectite precipitation upon reaction with CO_2-rich brines.[36] It is not known what impact smectite precipitation would have on the mechanical properties of the cement–caprock interface.

Our combined data set shows that wellbore permeability not only depends on changes in porosity due to portlandite dissolution, carbonate precipitation and dissolution, and the alteration of cement hydrates to an amorphous zeolite, but also on the mechanical properties of the altered layers. The strong interplay between cement alteration and their response to stress at the cement–caprock interface may explain both the development of such large reaction fronts and the observation that some wellbore cement is stable during CO_2 injection for decades.[6]

■ ASSOCIATED CONTENT

Supporting Information

Additional method details, two tables (brine composition and mineral fomula), and three figures (^1H NMR, ^{29}Si NMR, and a SEM image) are provide. This material is available free of charge via the Internet at http://pubs.acs.org.

■ AUTHOR INFORMATION

Corresponding Author

*Phone: 925-423-1041; e-mail: mason42@llnl.gov.

Notes

The authors declare no competing financial interest.

■ ACKNOWLEDGMENTS

This work was funded by the DOE, Office of Fossil Energy, National Risk Assessment Partnership. We would like to thank M. Smith for assistance with the initial setup of the core-flood experiment, S. Torres and D. Ruddle for preparation of sample cores, L. Knauer and the California Well Sample Repository for the caprock samples, D. Urabe for load testing, K. Fisher for ultrasonic testing, V. Genetti and R. Lindvall for ICP–MS meausement, and S. Kucheyev for assistance with nano-indentation measurements. We would also like to thank four anonymous reviewers for valuable comments that led to improvements in this work. This work was performed by LLNL under Contract DE-AC52-07NA27344. LLNL-JRNL-587375.

■ REFERENCES

(1) Watson, T. L.; Bachu, S. Evaluation of the potential for gas and CO_2 leakage along wellbores. *SPE Drill. Comp.* **2009**, *24* (1), 115–126.

(2) Kutchko, B. G.; Strazisar, B. R.; Dzombak, D. A.; Lowry, G. V.; Thaulow, N. Degradation of well cement by CO_2 under geologic sequestration conditions. *Environ. Sci. Technol.* **2007**, *41* (13), 4787–4792.

(3) Kutchko, B. G.; Strazisar, B. R.; Lowry, G. V.; Dzombak, D. A.; Thaulow, N. Rate of CO_2 attack on hydrated Class H well cement under geologic sequestration conditions. *Environ. Sci. Technol.* **2008**, *42* (16), 6237–6242.

(4) Kutchko, B. G.; Strazisar, B. R.; Huerta, N.; Lowry, G. V.; Dzombak, D. A.; Thaulow, N. CO_2 Reaction with hydrated class H

well cement under geologic sequestration conditions: Effects of flyash admixtures. *Environ. Sci. Technol.* **2009**, *43* (10), 3947−3952.
(5) Huerta, N. J.; Hesse, M. A.; Bryant, S. L.; Strazisar, B. R.; Lopano, C. L. Experimental evidence for self-limiting reactive flow through a fractured cement core: Implications for time-dependent wellbore leakage. *Environ. Sci. Technol.* **2012**.
(6) Carey, J. W.; Wigand, M.; Chipera, S. J.; WoldeGabriel, G.; Pawar, R.; Lichtner, P. C.; Wehner, S. C.; Raines, M. A.; Guthrie, G. D., Jr. Analysis and performance of oil well cement with 30 years Of CO_2 exposure from the SACROC Unit, West Texas, USA. *Int. J. Greenhouse Gas Control* **2007**, *1* (1), 75−85.
(7) Constantinides, G.; Ulm, F.; Van Vliet, K. On the use of nanoindentation for cementitious materials. *Mater. Struct.* **2003**, *36* (257), 191−196.
(8) Ulm, F. J. Chemomechanics of concrete at finer scales. *Mater. Struct.* **2003**, *36* (261), 426−438.
(9) Lewis, K.; Zyvoloski, G.; Keller, S.; Carey, J. W. Coupled stress and flow along interfaces in the wellbore environment in relation to CO_2 sequestration., In: 46th US Rock Mechanics Symposium, Chicago, IL, 2012; ARMA: Chicago, IL, 2012; pp 12−437.
(10) Settgast, R.; Johnson, S.; Fu, P.; Walsh, S. D.; Ryerson, F. Simulation of hydraulic fracture networks in three dimensions., In: 37th Workshop on Geothermal Reservoir Engineering, Stanford University, Stanford, CA, 2012; Stanford University: Stanford, CA, 2012; pp SGP-TR-194.
(11) Smith, M. M.; Sholokhova, Y.; Hao, Y.; Carroll, S. Evaporite caprock integrity: An experimental study of reactive mineralogy and pore-scale heterogeneity during brine-CO_2 exposure. *Environ. Sci. Technol.* **2012**.
(12) Walsh, S. D. C.; Du Frane, W. L.; Mason, H. E.; Carroll, S. A. Permeability of welbore-cement fractures following degredation by carbonated brines. *Rock Mech. Rock Eng.* **2012**, in press.
(13) Carroll, S. A.; Knauss, K. G. Dependence of labradorite dissolution kinetics on CO_2(aq), Al-(aq), and temperature. *Chem. Geol.* **2005**, *217* (3−4), 213−225.
(14) Wolery, T. W. *EQ3/6, A Software Package for Geochemical Modeling of Aqueous Systems*; Lawrence Livermore National Laboratory: Livermore, CA, 1992.
(15) Zhang, M.; Bachu, S. Review of integrity of existing wells in relation to CO_2 geological storage: What do we know? *Int. J. Greenhouse Gas Control* **2011**, *5* (4), 826−840.
(16) Cong, X. D.; Kirkpatrick, R. J. Si-29 MAS NMR study of the structure of calcium silicate hydrate. *Adv. Cement Based Mater.* **1996**, *3* (3−4), 144−156.
(17) Andersen, M. D.; Jakobsen, H. J.; Skibsted, J. Incorporation of aluminum in the calcium silicate hydrate (C-S-H) of hydrated Portland cements: A high-field ^{27}Al and ^{29}Si MAS NMR Investigation. *Inorg. Chem.* **2003**, *42* (7), 2280−2287.
(18) Houston, J. R.; Maxwell, R. S.; Carroll, S. A. Transformation of meta-stable calcium silicate hydrates to tobermorite: reaction kinetics and molecular structure from XRD and NMR spectroscopy. *Geochem. Trans.* **2009**, *10*, 1−14.
(19) Skibsted, J.; Henderson, E.; Jakobsen, H. J. Characterization of calcium aluminate phases in cements by ^{27}Al MAS NMR-spectroscopy. *Inorg. Chem.* **1993**, *32* (6), 1013−1027.
(20) Skibsted, J.; Jakobsen, H. J.; Hall, C. Quantitative aspects of ^{27}Al MAS NMR of calcium aluminoferrites. *Adv. Cement Based Mater.* **1998**, *7* (2), 57−59.
(21) Polak, A.; Elsworth, D.; Yasuhara, H.; Grader, A. S.; Halleck, P. M. Permeability reduction of a natural fracture under net dissolution by hydrothermal fluids. *Geophys. Res. Lett.* **2003**, *30* (20), 1647−1650.
(22) Smith, D. M.; Scherer, G. W.; Anderson, J. M. Shrinkage during drying of silica-gel. *J. Non-Cryst. Solids* **1995**, *188* (3), 191−206.
(23) Brown, P. W.; Doerr, A. Chemical changes in concrete due to the ingress of aggressive species. *Cem. Concr. Res.* **2000**, *30* (3), 411−418.
(24) Scherer, G. W.; Kutchko, B.; Thaulow, N.; Duguid, A.; Mook, B. Characterization of cement from a well at Teapot Dome Oil Field: Implications for geological sequestration. *Int. J. Greenhouse Gas Control* **2011**, *5* (1), 115−124.
(25) Mason, H. E.; Maxwell, R. S.; Carroll, S. A. The formation of metastable aluminosilicates in the Al−Si−H_2O system: Results from solution chemistry and solid-state NMR spectroscopy. *Geochim. Cosmochim. Acta* **2011**, *75* (20), 6080−6093.
(26) Yesinowski, J. P.; Eckert, H.; Rossman, G. R. Characterization of hydrous species in minerals by high-speed ^{1}H MAS NMR. *J. Am. Chem. Soc.* **1988**, *110* (5), 1367−1375.
(27) Liu, C. H. C.; Maciel, G. E. The fumed silica surface: A study by NMR. *J. Am. Chem. Soc.* **1996**, *118* (21), 5103−5119.
(28) Matteo, E. N.; Scherer, G. W. Experimental study of the diffusion-controlled acid degradation of Class H Portland cement. *Int. J. Greenhouse Gas Control* **2012**, *7*, 181−191.
(29) Van Cappellen, P.; Dixit, S.; van Beusekom, J. Biogenic silica dissolution in the oceans: Reconciling experimental and field-based dissolution rates. *Global Biogeochem. Cycles* **2002**, *16* (4), 1075.
(30) Carroll, S.; Mroczek, E.; Alai, M.; Ebert, M. Amorphous silica precipitation (60 to 120 degrees C): Comparison of laboratory and field rates. *Geochim. Cosmochim. Acta* **1998**, *62* (8), 1379−1396.
(31) Bickmore, B. R.; Nagy, K. L.; Gray, A. K.; Brinkerhoff, A. R. The effect of $Al(OH)_4^-$ on the dissolution rate of quartz. *Geochim. Cosmochim. Acta* **2006**, *70* (2), 290−305.
(32) Carey, J. W.; Svec, R.; Grigg, R.; Lichtner, P. C.; Zhang, J.; Crow, W., Wellbore integrity and CO_2-brine flow along the casing-cement microannulus. *Greenhouse Gas Control Technol. 9* **2009**, *1*, (1).
(33) Johnson, J. W.; Oelkers, E. H.; Helgeson, H. C. SUPCRT92—A software package for calculating the standard molal thermodynamic properties of minerals, gase, aqueous species, and reaction from 1-bar to 5000-bar and 0 to 1000 C. *Comput. Geosci.* **1992**, *18* (7), 899−947.
(34) CEMDATA Thermodynamic data for hydrated solids in Portland cement system (CaO-Al_2O_3-SiO_2-$CaSO_4$-$CaCO_3$-Fe_2O_3-MgO-H_2O). In http://www.empa.ch/cemdata.
(35) Neuhoff, P. S. *Thermodynamic Properties and Paragenesis of Rock-Forming Zeolites*; Stanford University Press: Stanford, CA, 2000.
(36) Carroll, S. A.; McNab, W. W.; Torres, S. C. Experimental Study of Cement−Sandstone/Shale−Brine−CO_2 Interactions. *Geochemical Transactions* **2011**, *12*.